ELSEVIER

Flow characteristics of water through a microchannel between two parallel plates with electrokinetic effects

Gh. Mohiuddin Mala and Dongqing Li
Department of Mechanical Engineering, University of Alberta, Edmonton, Alberta, Canada

C. Werner and H.-J. Jacobasch
Institute of Polymer Research, Dresden, Germany

Y. B. Ning
Alberta Microelectronic Center, Edmonton, Alberta, Canada

This paper investigates the interfacial electrokinetic effects on characteristics of liquid flow through a microchannel between two parallel plates. Experiments were conducted to investigate the effects of electric double layer (EDL) on flow characteristics with different potassium chloride concentrations in water and with different plate materials, P-type silicon, and glass. Microchannels with a height ranging from 10 ~ 280 μm were used in the measurement. A mathematical model was developed for steady-state liquid flow with the consideration of EDL effects. The predicted volume flow rates agree well with the measured data. The effects of the EDL field, the ionic concentration, and the channel size on the velocity distribution and friction factor are also discussed in this paper.

Keywords: microchannel flow; electric double layer; electrokinetic effects; zeta potential; streaming potential; friction coefficient; apparent viscosity

Introduction

Liquid flows through microchannels have wide industrial applications, such as design of microfluidic systems and microheat sinks. As characteristic dimensions of channels decrease to micro ranges, the fluid flow behavior in these microchannels is strongly influenced by the wall/interfacial effects. The flow characteristics are different from the normal situation described by the Navier–Stokes equations. For example, Eringen (1964) proposed a theory that states that fluid flow in microchannels will deviate from that predicted by Navier–Stokes equations. Tuckermann and Pease (1981, 1982) investigated experimentally and theoretically the fluid flow through microchannels. They found that the flow friction measurements were slightly higher than those predicted by the classical theories. Pfahler (1992) measured the friction coefficient in microchannels and found a significantly higher flow rate than expected for both isopropanol and silicon oil. His results indicate that polar nature of the fluid may play a role in the change in the observed viscosity. Choi et al. (1991) measured friction factor in microtubes of inside diameters 3 to 81 μm using nitrogen gas. They found that for diameters smaller than 10 μm, the friction coefficient C_f, product of the friction factor f and Reynolds number Re, was equal to 53 instead of 64. Harley and Bau (1989) measured the friction factor in channels of trapezoidal and square cross sections. They found experimentally that the friction coefficient C_f ranged from 49 for square channels to 512 for the trapezoidal channels. Peng et al. (1994a, 1994b) and Wang and Peng (1994) found experimentally that transition to turbulent flow began at Re = 200 to 700, and that fully turbulent connective heat transfer was reached at Re = 400 to 1500. They also observed that transitional Re diminished as the size of the microchannel decreased. Rice and Whitehead (1965) studied the effect of the surface electrical potential on liquid transport through narrow cylindrical capillaries with the assumption of the small surface electrical potential. Levine et al. (1975) extended the Rice and Whitehead model to higher surface electrical potential for flows in cylindrical capillaries.

In our previous work, Mala et al. (1997), the surface potential effects on flow characteristics in microchannels were studied theoretically. It was concluded that the effect of the electric double layer (EDL) on velocity distribution, friction coefficient, apparent viscosity, and heat transfer cannot be neglected in microscale fluid flow and heat transfer. Most solid surfaces bear electrostatic charges; i.e., an electrical surface potential. If the liquid contains very small amounts of ions, the electrostatic charges on the solid surface will attract the counterions in the

Address reprint requests to Dr. D. Li, Department of Mechanical Engineering, University of Alberta, Edmonton, Alberta, Canada.

Received 18 December 1996; accepted 5 March 1997

Int. J. Heat and Fluid Flow 18: 489–496, 1997

655 Avenue of the Americas, New York, NY 10010

0142-727X/97/$17.00
PII S0142-727X(97)00032-5

liquid to establish an electrical field. The arrangement of the electrostatic charges on the solid surface and the balancing charges in the liquid is called the EDL. The EDL is composed of the compact layer and diffuse double layer. The compact layer is about 0.5-mm thick. In the compact layer, the ions are strongly attracted to the wall surface and are immobile. In diffuse double layer, the ions are affected less by the electrical field and are mobile. The thickness of the diffuse EDL generally ranges from a few nanometers up to several hundreds of nanometers, depending upon the electric potential of the solid surface, the bulk ionic concentration, and other properties of the liquid. The electrical potential at the boundary between the compact layer and the diffuse layer is called the zeta potential ξ.

When a liquid is forced through a microchannel under hydrostatic pressure, the ions in the mobile part of the EDL are carried towards one end. This causes an electrical current, the streaming current, to flow in the direction of the liquid flow. The accumulation of ions downstream sets up an electrical field with an electrical potential, the streaming potential. This field causes a current, the conduction current, to flow back in the opposite direction. When conduction current equals streaming current, a steady state is reached. It is easy to understand that, when the ions are moved in the diffuse double layer, they pull the liquid along with them. The motion of the ions in the diffuse double layer is subject to the electrical potential of the double layer and the streaming potential. Thus, liquid flow characteristics are affected by the presence of EDL.

In macroscale flow, interfacial electrokinetic effects are negligible, because the thickness of the EDL is negligible compared to the hydraulic radius of the flow channel. However, in microscale flow, the EDL thickness may be comparable to the hydraulic radius of the flow channel. For pure water and pure oils, the thickness of EDL can be as large as several microns. Thus, EDL effect will be significant for flows in small microchannels. An experimental study of EDL effects on microchannel flows was undertaken recently and is reported in this paper. The experimental results are compared with the results obtained from the developed mathematical model. A good agreement between the experimental and computed results has been found.

Mathematical model

The mathematical model characterizing the fluid flow through a microchannel between two parallel plates with the effects of EDL is described in the following sections.

Poisson–Boltzmann equation

Consider a fluid phase containing positive and negative ions in contact with a planar positively or negatively charged surface. An EDL field will be established. Assume that the surface bears a uniform electrostatic potential, which decreases as one proceeds out into the fluid. Far away from the wall, the concentration of the positive and negative ions is equal. The electrostatic potential ψ, at any point near the surface, is related to the net number of electrical charges per unit volume ρ, in the neighborhood of the point, which measures the excess of the positive ions over negative ions or vice versa. According to the theory of electrostatics, the relation between ψ and ρ is given by Poisson's equation (Hunter 1981), which for a flat surface is

$$\frac{d^2\psi}{dX^2} = -\frac{\rho}{\varepsilon_o \varepsilon} \tag{1}$$

Notation

A_c cross-sectional area of the flow channel, m^2
C_f friction coefficient, (f*Re) dimensionless
E_s streaming potential, V
E_z electric field strength, $V\ m^{-1}$
I_c, I_s conduction and streaming currents respectively, A
P_s wetted perimeter of the channel, m
P_z pressure gradient in z-direction $= -dp/dZ$, Pa m^{-1} (N/m^{-3})
Q volume flow rate through the channel, $m^3\ s^{-1}$
Q_p conventional volume flow rate through the channel, $m^3\ s^{-1}$
R_b bulk electrical resistance of the liquid flowing in the channel, Ω
Re Reynolds number, dimensionless
R_s surface electrical resistance of the channel, Ω
R_T total electrical resistance of the channel with the liquid, Ω
T absolute temperature, K
V_{av} average velocity of the fluid, $m\ s^{-1}$
V_o reference velocity (arbitrarily chosen as $1m\ s^{-1}$)
V_z velocity of the fluid in Z-direction $m\ s^{-1}$
X X-coordinate, m
Z Z-coordinate, m
a half of the separation distance between the two plates, m
e electron charge, $1.6021 \times 10^{-19}\ C$
f friction factor, dimensionless
k Debye–Huckel parameter, $(2n_o z^2 e^2/\varepsilon\varepsilon_o k_b T)^{1/2}\ m^{-1}$
k_b Boltzmann constant, $1.3805 \times 10^{-23}\ J\ mol^{-1}\ K^{-1}$
l length of the channel, m
n^+, n^- concentration of positive and negative ions, m^{-3}
n_o average number of positive or negative ions/unit volume or ionic number concentration, m^{-3}
z^+, z^- valence of the positive and negative ions

Greek

ε dielectric constant of the medium, dimensionless
ε_o permittivity of vacuum, $8.854 \times 10^{-12}\ C\ V^{-1}\ m^{-1}$
κ nondimensional electrokinetic separation distance between the two plates (a*k)
λ_b bulk conductivity of the fluid, $\Omega^{-1}\ m^{-1}$
λ_s surface conductivity of the channel wall, Ω^{-1}
λ_T total conductivity of the fluid, $\Omega^{-1}\ m^{-1}$
μ dynamic viscosity of the fluid, $Ns\ m^{-2}$
μ_a apparent viscosity of the fluid, $Ns\ m^{-2}$
ξ zeta potential; i.e., the electric potential at the boundary between the diffuse double layer and the compact layer, V
ρ charge density, $C\ m^{-3}$
ρ_f density of fluid, $kg\ m^{-3}$
τ_w shear stress at the channel wall, $N\ m^{-2}$
ψ electrostatic potential at any point in the electric double layer, V

Subscript

- nondimensional parameters

The probability of finding an ion at a particular point is proportional to the Boltzmann factor $e^{-ze\psi/k_bT}$. For any fluid consisting of two kinds of ions of equal and opposite charge z^+, z^-, the number of ions of each type are given by the Boltzmann equation (Hunter 1981)

$$n^- = n_o e^{ze\psi/k_bT} \quad \text{and} \quad n^+ = n_o e^{-ze\psi/k_bT}$$

The net charge density in a unit volume of the fluid is given by

$$\rho = (n^+ - n^-)ze = -2n_o ze \sinh(ze\psi/k_bT) \tag{2}$$

Substituting Equation 2 in Equation 1, we obtain a nonlinear second-order one-dimensional (1-D) Poisson–Boltzmann equation.

$$\frac{d^2\psi}{dX^2} = \frac{2n_o ze}{\varepsilon_o \varepsilon} \sinh\left(\frac{ze\psi}{k_bT}\right) \tag{3}$$

Nondimensionalizing equations 1 and 3 via

$$\bar{X} = \frac{X}{a}, \quad \bar{\psi} = \frac{ze\psi}{k_bT}, \quad \text{and} \quad \bar{\rho}(\bar{X}) = \frac{\rho(X)}{n_o ze} \tag{4}$$

We obtain the nondimensional forms of Equations 1 and 3 after some simplification as:

$$\frac{d^2\bar{\psi}}{d\bar{X}^2} = -\frac{\kappa^2}{2}\bar{\rho}(\bar{X}) \tag{5}$$

$$\frac{d^2\bar{\psi}}{d\bar{X}^2} = \kappa^2 \sinh(\bar{\psi}) \tag{6}$$

Where $k = (2n_o z^2 e^2/\varepsilon\varepsilon_o k_b T)^{1/2}$ and $(a^*k) = \kappa$. "k" is called the Debye–Huckel parameter, while "$1/k$" is referred to as the characteristic thickness of the EDL. As explained earlier, the characteristic thickness of the EDL can vary from few nanometers to a micrometer, depending upon the solid-liquid system.

Solution of the Poisson–Boltzmann equation

If the electrical potential is small compared to the thermal energy of the ions; i.e., $(|ze\psi| < |k_bT|)$ so that the exponential in Equation 6 can be approximated by the first terms in a Taylor series. This transforms Equation 6 into

$$\frac{d^2\bar{\psi}}{d\bar{X}^2} = \kappa^2\bar{\psi} \tag{7}$$

In the literature, this is called the Debye–Huckel linear approximation (Hunter 1981). The solution of the above equation can be obtained easily. Consider a flow channel between two parallel plates, as shown in Figure 1 . If the electrical potential of the channel surface is small, and the separation distance between the two plates is larger than the thickness of the EDL so that the EDLs near the two plates will not overlap, the appropriate boundary conditions are: at $\bar{X} = 0, \bar{\psi} \approx 0$ and at $\bar{X} \approx \pm 1, \bar{\psi} = \bar{\xi} = (ze\xi/k_bT)$. With these boundary conditions, the solution of Equation 7 is obtained and is given by

$$\bar{\psi} = \frac{\bar{\xi}}{\sinh(\kappa)} |\sinh(\kappa\bar{X})| \tag{8}$$

Equation of motion

Consider a 1-D fully developed, steady-state, laminar flow through two parallel plates of unit width, as shown in Figure 1. The forces acting on an element of fluid include the pressure force, the viscous force, and the electric body force generated by the double-layer electric field. The equation of motion is the Z-directional momentum equation.

$$\mu\frac{d^2V_z}{dX^2} + P_z + E_z\rho(X) = 0 \tag{9}$$

where $E_z = E_s/l$ and $P_z = -dp/dZ$. $E_z\rho(X)$ is the electrical body force. Nondimensionalize Equation 9 with $\bar{E}_s = E_s/\xi$, $\bar{V}_z = V_z/V_o$ and replace $\bar{\rho}(\bar{X})$ from Equation 5, we obtain

$$\frac{d^2\bar{V}_z}{d\bar{X}^2} + G_1 - \frac{2G_2\bar{E}_s}{\kappa^2}\frac{d^2\bar{\psi}}{d\bar{X}^2} = 0$$

where the two nondimensional numbers are $G_1 = (a^2P_z/\mu V_o)$ and $G_2 = (\xi n_o zea^2/l\mu V_o)$. Integrating Equation 10 twice we get

$$\bar{V}_z + \frac{G_1\bar{X}^2}{2} - \frac{2G_2\bar{E}_s}{\kappa^2}\bar{\psi} = C_1\bar{X} + C_2$$

The constants of integration C_1 and C_2 can be found by employing the appropriate boundary conditions; namely, at $\bar{X} = \pm 1$, $\bar{V}_z = 0$, $\bar{\psi} = \bar{\xi}$. After evaluating the constants C_1 and C_2 the velocity distribution is given by

$$\bar{V}_z = \frac{G_1}{2}(1 - \bar{X}^2) - \frac{2G_2\bar{E}_s\bar{\xi}}{\kappa^2}\left\{1 - \frac{\bar{\psi}}{\bar{\xi}}\right\} \tag{10}$$

Substituting for $\bar{\psi}$ from Equation 8 the nondimensional velocity distribution is:

$$\bar{V}_z = \frac{G_1}{2}(1 - \bar{X}^2) - \frac{2G_2\bar{E}_s\bar{\xi}}{\kappa^2}\left\{1 - \left|\frac{\sinh(\kappa\bar{X})}{\sinh(\kappa)}\right|\right\} \tag{11}$$

Streaming potential

As seen from Equation 11, the velocity distribution can be calculated only if the streaming potential $\bar{E}_s$ is known. In the absence of an applied electric field, when a liquid is forced through a channel under hydrostatic pressure an electrical field is generated as explained in the introduction. The potential of this electrical field is called the streaming potential. The current attributable to the transport of charges by the liquid flow, called

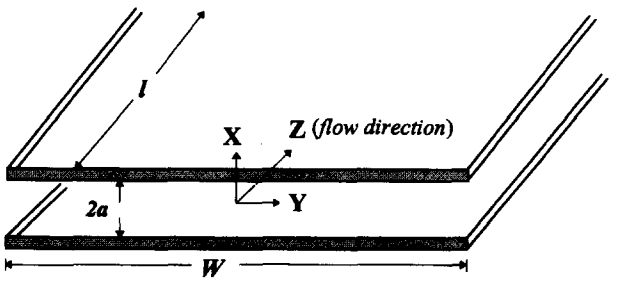

Figure 1 Schematic of a microchannel between two parallel plates

streaming current, is given by

$$I_s = \int_{A_c} V_z \rho(X)\, dA_c \tag{12}$$

Nondimensionalizing V_z and $\rho(X)$ we obtain

$$\bar{I}_s = \frac{I_s}{2n_o V_o zea} = \int_0^1 \bar{V}_z \bar{\rho}(\bar{X})\, d\bar{X} \tag{13}$$

Substituting for $\bar{\rho}(\bar{X})$ from Equation 5, the nondimensional streaming current becomes

$$\bar{I}_s = -\frac{2}{\kappa^2}\int_0^1 \bar{V}_z\, d\left(\frac{d\bar{\psi}}{d\bar{X}}\right) = \bar{V}_z \frac{d\bar{\psi}}{d\bar{X}}\bigg|_0^1 - \int_0^1 \frac{d\bar{\psi}}{d\bar{X}}\, d\bar{V}_z \tag{14}$$

With the boundary conditions; namely $\bar{X}=1$, $\bar{V}_z = 0$ and $\bar{X}=0$, $d\bar{\psi}/d\bar{X} = 0$, the first term on right-hand side of Equation 14 becomes zero. Therefore, the streaming current reduces to

$$\bar{I}_s = \frac{2}{\kappa^2}\int_0^1 \frac{d\bar{\psi}}{d\bar{X}}\, d\bar{V}_z \tag{15}$$

Using Equation 10, Equation 15 can be written as:

$$\bar{I}_s = \frac{2}{\kappa^2}\left[-G_1\int_0^1 \bar{X}\, d\bar{\psi} + \frac{2G_2\bar{E}_s}{\kappa^2}\int_0^1 \left(\frac{d\bar{\psi}}{d\bar{X}}\right)^2 d\bar{X}\right]$$

the integrals are evaluated by using Equation 8 and are given as

$$\int_0^1 \bar{X}\, d\bar{\psi} = \bar{\xi}\left(1 - \frac{\cosh(\kappa)-1}{\kappa\sinh(\kappa)}\right)$$

$$\int_0^1 \left(\frac{d\bar{\psi}}{d\bar{X}}\right)^2 d\bar{X} = \left(\frac{\kappa\bar{\xi}}{\sinh(\kappa)}\right)^2\left(\frac{\sinh(\kappa)\cosh(\kappa)}{2\kappa} + \frac{1}{2}\right)$$

Finally the nondimensional streaming current is given by

$$\bar{I}_s = -\frac{2G_1\bar{\xi}\beta_1}{\kappa^2} + 4G_2\bar{E}_s\beta_2\left(\frac{\bar{\xi}}{\kappa\sinh(\kappa)}\right)^2$$

where

$$\beta_1 = 1 - \frac{\cosh(\kappa)-1}{\kappa\sinh(\kappa)} \quad \text{and} \quad \beta_2 = \frac{\sinh(\kappa)\cosh(\kappa)}{2} + \frac{1}{2} \tag{16}$$

The streaming potential generated by the streaming current will produce a conduction current in the reverse direction, and is given by

$$I_c = \frac{\lambda_b E_s A_c}{l} + \frac{\lambda_s E_s P_s}{l} \tag{17}$$

where λ_b and λ_s are the bulk and surface conductivity respectively. I_c can be rewritten as

$$I_c = \frac{E_s A_c \lambda_T}{l}$$

$$\lambda_T = \lambda_b + \frac{\lambda_s P_s}{A_c} \tag{18}$$

Nondimensionalizing as before with $\bar{l} = l/a$, the nondimensional conduction current is

$$\bar{I}_c = \frac{I_c}{\xi\lambda_T a} = \frac{\bar{E}_s \bar{A}_c}{\bar{l}} \tag{19}$$

At a steady state, there will be no net current in the flow; i.e., $I_c + I_s = 0$. Using I_c from Equation 19 and I_s from Equation 13 we obtain after some simplification $\bar{I}_c + (2V_o n_o ze/\xi\lambda_T)\bar{I}_s = 0$.

Substituting for $\bar{I}_c$ and $\bar{I}_s$ from Equation 19 and Equation 16 the streaming potential is obtained.

$$\bar{E}_s = \frac{2G_1G_3\bar{\xi}\beta_1}{\kappa^2 + 4\beta_2G_2G_3[\bar{\xi}/\sinh(\kappa)]^2} \tag{20}$$

Where the nondimensional factor $G_3 = V_o n_o zel/\xi\lambda_T$.

In the classical theory of electrokinetic flow, the effect of EDL on the liquid flow and the effects of surface conductance are not considered. The streaming potential is related to the zeta potential and liquid properties through the following Equation (Hunter 1981).

$$\frac{E_s}{\Delta P} = \frac{\varepsilon\varepsilon_o\xi}{\mu\lambda_b} \tag{21a}$$

Equation 20 can be rearranged in a form similar to Equation 21a by substituting back the values of the nondimensional parameters; i.e.,

$$\frac{E_s}{\Delta P} = \frac{\varepsilon\varepsilon_o\xi}{\mu\lambda_T}\Phi \tag{21}$$

Where the correction factor Φ to the classical theory is given as

$$\Phi = \frac{\beta_1}{1 + \dfrac{\beta_2\kappa^2\varepsilon^2\varepsilon_o^2\xi^2}{\sinh^2(\kappa)a^2\mu\lambda_T}} \tag{22}$$

If $\Phi = 1$ and $\lambda_T = \lambda_b$, Equation 21 becomes the classical equation.

Volume flow rate and apparent viscosity

The volume flow rate through the parallel plates can be obtained by integrating the velocity distribution over the cross-sectional area, as

$$Q = \int_{A_c} V_z\, dA_c \tag{23}$$

Using Equation 11, the volume flow rate in nondimensional form is

$$\bar{Q} = \frac{2G_1}{3} - \frac{4G_2\bar{E}_s\bar{\xi}}{\kappa^2} + \frac{4G_2\bar{E}_s\bar{\xi}}{\kappa^3}\frac{(\cosh(\kappa)-1)}{\sinh(\kappa)} \tag{24}$$

For steady flow under an applied pressure gradient (without an externally applied electric field), the volume flow rate is given by Equation 24. This reduced rate of flow will result in an apparent viscosity μ_a ($> \mu$), so that the conventional form of volume flow rate for flow between two parallel plates separated by a distance "$2a$" is

$$Q_p = \frac{2P_z a^3}{3\mu_a} \tag{25}$$

If the EDL effect is negligible, $\mu_a = \mu$, then Equation 25 becomes the classical Poiseuille volume flow rate equation. Nondimensionalizing Equation 25, the volume flow rate is

$$\bar{Q}_p = \frac{2G_1\mu}{3\mu_a} \tag{26}$$

Equalizing Equation 24 with Equation 26; i.e., $\bar{Q} = \bar{Q}_p$, we obtain the ratio of the apparent viscosity to the true bulk viscosity:

$$\frac{\mu_a}{\mu} = \frac{\kappa^3 G_1}{\kappa^3 G_1 - 6G_2\bar{E}_s\bar{\xi}\kappa + 6G_2\bar{E}_s\bar{\xi}(\cosh(\kappa) - 1)/\sinh(\kappa)} \tag{27}$$

Friction coefficient

The friction coefficient C_f is the product of the friction factor f and Re. The friction factor and the Re number for the flow between two parallel plates with a separation distance "$2a$" is given by

$$f = \frac{8\tau_w}{\rho_f V_{av}^2} \quad \text{and} \quad \text{Re} = \frac{\rho_f V_{av} a}{\mu}$$

Where $V_{av} = Q/A_c$. The shear stress is given by

$$\tau_w = \left|\mu \frac{dV_z}{dX}\right|_{X=\pm a} = \left|\frac{\mu V_o}{a}\frac{d\bar{V}_z}{d\bar{X}}\right|_{\bar{X}=\pm 1}$$

Differentiating Equation 11 once for $(d\bar{V}_z/d\bar{X})$, we obtain the friction coefficient C_f as

$$C_f = f\,\text{Re} = \frac{8V_o}{V_{av}}\left(G_1 + \frac{2G_2\bar{E}_s\bar{\xi}}{\kappa}\coth(\kappa)\right) \tag{28}$$

Experiments

The measurement of electrokinetic effects on liquid flows through microchannels between two parallel plates were conducted by using an electrokinetic analyzer (EKA) (A. Paar GmbH, Graz, Austria). Primary parameters measured by EKA were the pressure drop and the electrical potential across a channel (the streaming channel) through which a testing aqueous electrolyte solution flows. The measured electrical potential is the streaming potential. The streaming channels were made of the material to be investigated. In this study, the solid plates used to form the microchannels were P-type silicon and 0211-glass. All solid plates were 10-mm wide and 20-mm long. In each experiment, a pair (either silicon or glass) of plates were mounted parallel in a specially designed measuring cell (Institute of Polymer Research, Dresden, Germany) to form the streaming channel.

Aqueous KCl solutions of several different concentrations and millipore water were used in the measurements. The EKA performs the measurements automatically. In each measurement, a closed tubing circuit and a gearwheel pump circulate an electrolyte solution through the streaming channel under a constant pressure difference. The constant pressure difference (between 20 and 350 mbar) is kept for at least 60 s to ensure a steady state of the flow. The streaming potential is measured when the steady state is reached. Temperature, pH, volume flow rate, conductance of the solution, and the total electrical resistance of the streaming channel are also measured in each measurement. For a given pressure, a given channel height, and a given ionic concentration, the above described measurement were repeated at least three times. The accuracy of the measured data is better than 1%. All measurements were taken at 25°C.

Data analysis

The measured data included the total electric resistance of the microchannels, the pressure drop, bulk conductivity, streaming potential, and flow rate.

Calculation of $\lambda_s P_s$

The product $\lambda_s P_s$ can be calculated from the measured electrical resistances from the following equation $(1/R_T) = [(1/R_b) + (1/R_s)]$. The surface and bulk electrical resistances in the above equation are given by $[(1/R_s) = (\lambda_s P_s/l)]$ and $[(1/R_b) = (\lambda_b A_c/l)]$, respectively. Thus, rearranging the above equation yields

$$\lambda_s P_s = l\left(\frac{1}{R_T} - \frac{\lambda_b A_c}{l}\right) \tag{29}$$

The total resistance R_T of the channel and the bulk conductivity λ_b are measured directly in the experiments. Once $\lambda_s P_s$ is known, the total conductivity λ_T can be calculated from Equation 18. Note that $\lambda_s P_s$ is constant for a given solid-solution system.

Determination of channel height and zeta potential

In this experiment it is difficult to measure accurately the distance between the plates; i.e., the channel height $2a$. If there is no (or negligible) EDL effect on the liquid flow, then the channel height can easily be determined from the measured volume flow rate by using the Poiseuille flow rate equation, Equation 25. This is the case for high concentration solutions or large flow channels, where the effect of the EDL is negligible. In the case of infinitely diluted solutions, like millipore water, the EDL and surface conductivity effects are significant. In this case, the flow rate is given by Equation 24. Equation 24 can be used to compute the actual channel height using two sets of experimental data of volume flow rate, pressure drop, and streaming potential for a fixed microchannel height and solution concentration. For example, for millipore water flowing through a silicon channel, two volume flow rates Q_1 and Q_2 corresponding to $\Delta P = 15$ kPa and $\Delta P = 35$ kPa are measured as 1.04×10^{-7} m^3/s and 2.75×10^{-7} m^3/s, respectively. The corresponding streaming potentials are measured to be $E_{s1} = -0.4065$ V and $E_{s2} = -0.68705$ V. Once E_s, ΔP, and Q are known, Equation 24 has two unknowns, the zeta potential ξ, and the half channel height a (involved in the parameter κ). We should realize the fact that for a given solution and the solid plates (the channel walls) system, ξ is a constant, independent of the pressure difference and the channel height. Therefore, by equating ξ in the two flow-rate equations,

Q_1 and Q_2, the half-channel height can be determined by

$$a = \left(\frac{3l\mu}{2w} \frac{E_{s1}Q_2 - E_{s2}Q_1}{E_{s1}\Delta P_2 - E_{s2}\Delta P_1} \right)^{\frac{1}{3}} \tag{30}$$

where w is the channel width.

From Equation 30, the channel height in the above example is 60.65 μm. This value of channel height is used to calculate the ξ potentials from Equation 24. For a given solution and the solid plate system, only one channel height and the zeta potential are determined by using the flow-rate Equation 24, as described above. Because once the zeta potential is known, the channel heights in all other cases of the same solid–liquid system can be determined from Equation 21 by using the measured E_s, ΔP and the liquid properties.

Total resistance, streaming potential and zeta potential

Figure 2 shows the variation of the measured total electrical resistance with the channel height for both P-type silicon and glass. For high ionic concentrations, the resistance decreases as the channel height increases for the silicon channels; whereas, it remains approximately constant for the glass channels. For millipore water, however, the resistance remains approximately same for the silicon channels but decreases for the glass channels. The resistance is much higher for glass surfaces than silicon surfaces, as shown in the figure.

Figure 3 shows the variation of the measured streaming potential E_s with channel height for various ionic concentrations, and channel materials. It is observed that for millipore water, the streaming potential decreases rapidly as the channel height increases. The rate of decrease is more for glass than for P-type silicon. For solutions with higher concentrations, the streaming potential remains approximately constant, independent of the channel material and the channel height.

Figure 4 shows the variation of ξ with ionic concentration for silicon and glass surfaces. It is found that by considering the surface conductivity effect the values of ξ are significantly higher at low concentrations, especially for millipore water. For P-type silicon, $\xi = 12mv$ is obtained from the classical theory; i.e.,

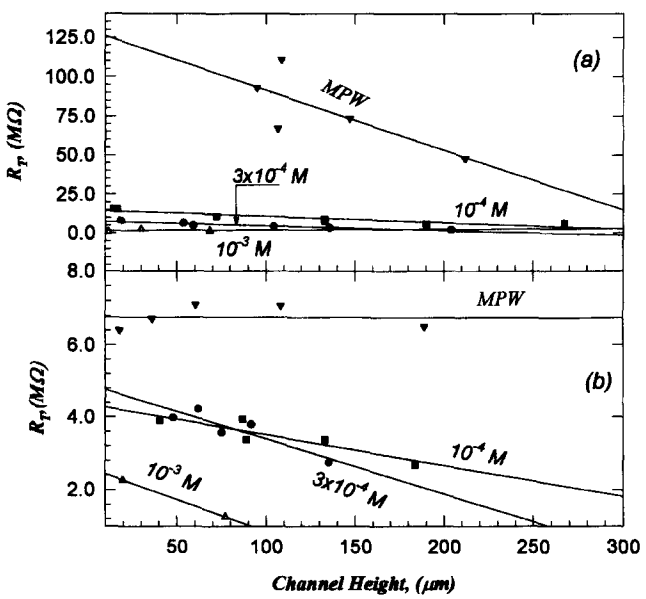

Figure 2 Variation of the channel's total electrical resistance with the channel height; (a) glass; and (b) silicon channels

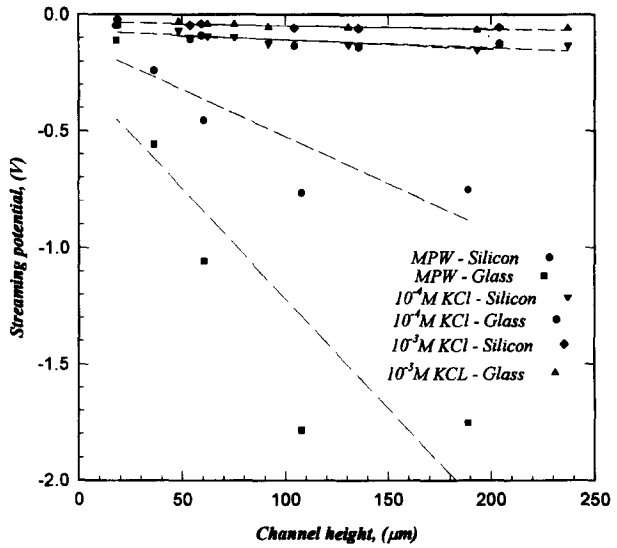

Figure 3 Variation of streaming potential with channel height for various solution concentrations and channel materials

Equation 21a, which does not consider the effect of surface conductivity and the EDL effect on flow. This value of ξ is significantly lower than $\xi = 200.7mv$, obtained from Equation 21, which considers the effects of surface conductivity and the EDL effect on flow. Therefore, to estimate the correct value of ξ for solutions with low ionic concentrations, the EDL effect on flow and the surface conductivity should always be considered.

Correction factor Φ

The correction factor Φ given by Equation 22, is computed for millipore water. Figure 5 shows the variation of Φ with channel height. For high concentration solutions, the value of electrokinetic separation distance κ ($\kappa = a^*k$) is very large. This makes β_1 and the denominator of Equation 22 approach unity as the concentration increases; therefore, Φ = 1 for highly concentrated

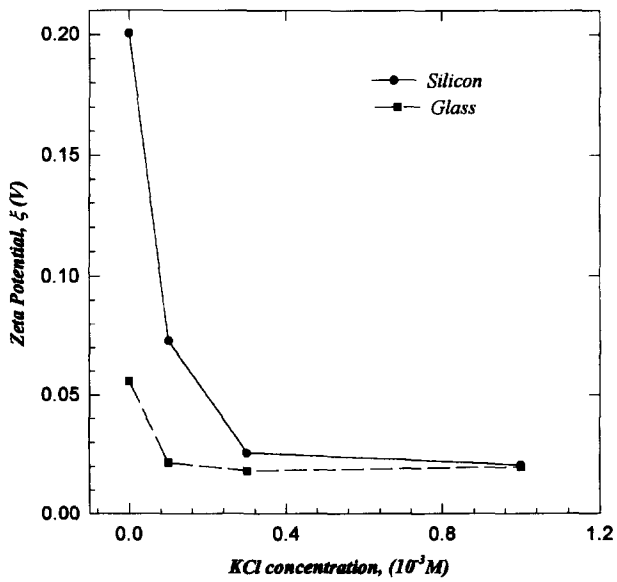

Figure 4 Zeta potential variation with ionic concentration for silicon and glass

solutions. For millipore water that is infinitely diluted, κ value is smaller, and the values of Φ are significantly lower than unity. As can be seen from Figure 5, for silicon channels, Φ changes from 0.69 to 0.97 as the channel height increases; however, for glass channels, the values of Φ are much higher ranging from 0.91 to 0.98. This is because the silicon channels have higher zeta potential and lower total electrical resistance of the channel with the liquid than that of glass channels, as shown in Figures 2 and 4. Therefore, the classical equation (Equation 21a) holds only for highly concentrated solutions, and the correction should be applied if working with diluted solutions and "pure" liquids.

Volume flow rate

The volume flow rates have been measured in the experiments. To verify the model developed in this paper, the measured flow rates are compared with the prediction of Equation 24. Equation 24 gives the reduced volume flow rate attributable to presence of the EDL field. If the EDL effect is negligible, as in the case of high ionic concentration solutions, then the second and third terms of right-hand side of Equation 24 vanish, resulting in the classical Poiseuille flow equation. Therefore, only millipore water's flow rates are compared with the predictions of Equation 24, as plotted in Figures 6a and 6b, as a function of channel height and different pressure drop. It can be seen that the volume flow rates obtained experimentally and the theoretical predictions are in good agreement with each other. This indicates that the mathematical model developed in this study is correct. In Figure 6c, the difference between the class and reduced-volume flow rates is shown. The difference is larger for silicon surfaces than for the glass surfaces. Also, as the channel height increases, the difference between the classic and reduced-volume flow rates decreases, more so for silicon than for glass. This is because the silicon surface has a higher zeta potential and surface conductivity than the glass surface.

Velocity distribution

The nondimensional velocity distribution $\bar{V}_z$ in the microchannels can be computed by using Equation 11 and the data of the streaming potential E_s, zeta potential ξ, and the channel height. Figure 7 shows the nondimensional velocity distribution for a 20-μm silicon channel with millipore water as the working fluid for two values of ΔP. As can be seen from the figure, the velocity profiles are parabolic, and as ΔP increases, the velocity increases. For the same values of ΔP the velocity is higher if $\xi = 0$ V; i.e., the EDL effect is absent, as compared to when the EDL effect is considered; i.e., for a finite value for ξ. Thus, EDL effect results in a lower velocity compared to that obtained by conventional theory.

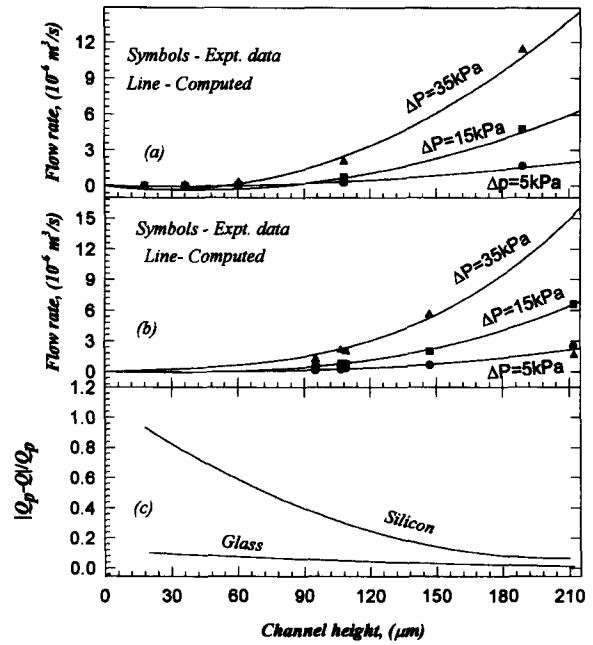

Figure 6 A comparison of volume flow rate of millipore water between: (a) experimental data and the predictions of Equation 24 in silicon channels; (b) experimental data and the predictions of Equation 24 in glass channels; and, (c) the predictions of Equation 26 and of Equation 24.

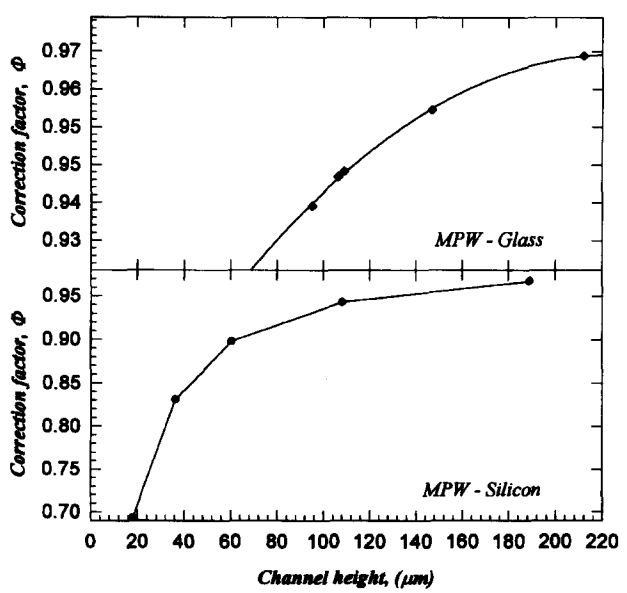

Figure 5 Variation of Φ with channel height for silicon and glass channels with millipore water as the working fluid

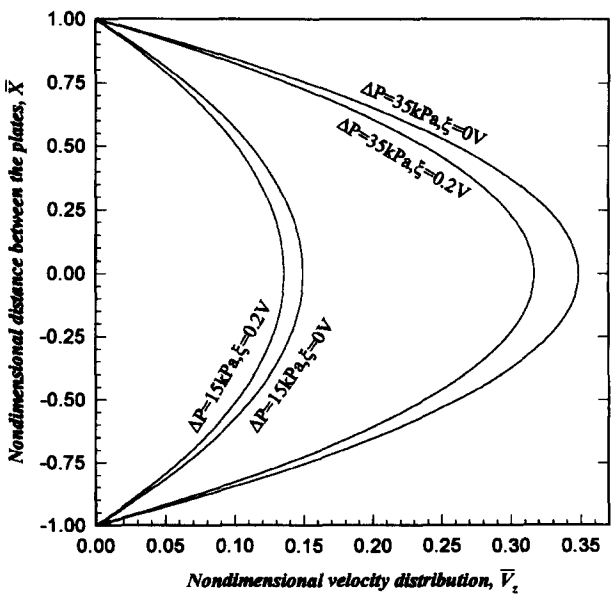

Figure 7 Nondimensional velocity distribution of millipore water in a 20 μm channel for various ΔP and ξ

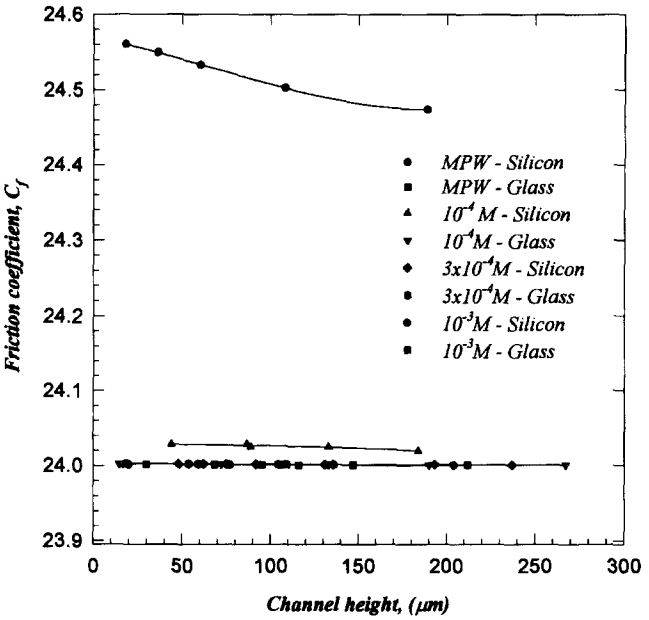

Figure 8 Variation of friction coefficient with channel height

Friction coefficient

The product of the friction factor f and Re as given by Equation 28 was computed for various values of ξ ($20 \sim 200$ mV). We know from classical theory (no EDL effect) that $C_f = 24$ for channels between two parallel plates. Using Equation 28 and the measured experimental data, C_f is calculated and is shown in Figure 8. For the case of small values of ξ and high ionic concentrations, the friction coefficient C_f is approximately 24. But as ξ increases and the ionic concentration decreases, C_f also increases. For $\xi = 200$ mV with millipore water as the working fluid $C_f = 24.56$. This may be understood as follows. As a liquid is forced through a microchannel under a pressure gradient, the charges in the mobile part of the double layer are carried to the downstream, and a streaming potential is established. This potential produces a backflow of ions and, hence, the liquid. The net result is a reduced flow in the forward direction. The liquid seems to exhibit an enhanced viscosity called apparent viscosity, if the flow rate is compared with the flow rate in the absence of the double-layer effects. This apparent viscosity results in a higher friction coefficient. When the ionic concentration increases, the EDL field will be compressed; i.e., the thickness of EDL field will be reduced. Therefore, the value of friction coefficient is closer to 24 at higher ionic concentrations. For a given ionic concentration, the higher the ξ values, the stronger the EDL effect on flow, and hence, the higher the friction coefficient value. As the channel height increases the friction coefficient value approach the conventional value of $C_f = 24$, as shown in the figure. These results are qualitatively in agreement with the results obtained by Peng et al. (1994a) in their experiments through rectangular microchannels.

Conclusion

The effect of EDL at the solid–liquid interface on liquid flows through a microchannel between two parallel plates were studied experimentally and theoretically. Generally, the EDL near the channel wall tends to restrict the motion of ions and, hence, the liquid molecules in the diffuse EDL region. The induced streaming potential drives the ions and, hence, the liquid molecules to move in the opposite direction to the flow. The following conclusions can be drawn:

(1) For solutions with high ionic concentrations, the thickness of the electrical double layer (characterized by the Debye–Huckel parameter; i.e., $1/k$) is very small, normally a few nanometers. Therefore, the EDL effects on flow in microchannels are negligible. However, for infinitely diluted solutions such as the millipore water used in this study, the thickness of the EDL is considerably large (about 1 μm). Therefore, the EDL effects on flows in microchannels become insignificant.

(2) The theory developed in this work can describe the flow characteristics in microchannels, as supported by the good agreement between the flow rates measured in the experiments and that predicted by the theory. Overall, the volume flow rates for millipore water are significantly lower than that predicted by the conventional fluid dynamics theory attributable to the EDL effects. The friction coefficient for flows in microchannels will increase as the zeta potential increases and as the ionic concentration decreases. However, from the experimental data and our model calculations, for microchannels with hydraulic diameters greater than few hundred micrometers, the EDL effect would be negligible.

Acknowledgments

The authors acknowledge the support of an Alberta Microelectronic Center Fellowship (Gh. Mohiuddin Mala) and the Natural Science and Engineering Research Council of Canada Research Grants (D. Li).

References

Choi, S. B., Barron, R. F. and Warrington, R. O. 1991. Fluid flow and heat transfer in microtubes. *ASME Proc.*, **32**, 123–134

Eringen, A. 1964. Simple microfluids. *Int. J. Eng. Sci.*, **2**, 205–217

Harley, J. and Bau, H. 1989. Fluid flow in micron and submicron size channel. *IEEE Trans.*, THO249-3, 25–28

Hunter, R. J. 1981. *Zeta Potential in Colloid Science: Principles and Applications*. Academic Press, New York

Levine, S., Marriott, J. R., Neale, G. and Epstein, N. 1975. Theory of electrokinetic flow in fine cylindrical capillaries at high zeta potential. *J. Colloid Sci.*, **52**, 136–149

Mala, G. M., Li, D. and Dale, J. D. 1997. Heat transfer and fluid flow in microchannels. *Int. J. Heat Mass Transfer* **40** (13) 3079–3088

Peng, X. F., Peterson, G. P. and Wang, B. X. 1994a. Frictional flow characteristics of water flowing through rectangular microchannels. *Exp. Heat Transfer*, **7**, 249–264

Peng, X. F., Peterson, G. P. and Wang, B. X. 1994b. Heat transfer characteristics of water flowing through microchannel. *Exp. Heat Transfer*, **7**, 265–283

Pfahler, J. N. 1992. Liquid transport in micron and submicron channels. Ph.D. thesis, University of Pennsylvania, Philadelphia, PA

Rice, C. L. and Whitehead, R. 1965. Electrokinetic flow in narrow cylindrical capillaries. *J. Phys. Chem.*, **69**, 4017–4023

Tuckermann, D. B. and Pease, R. F. W. 1981. High-performance heat sinks for VLSI. *IEEE Electron Device Lett.* **2**, 126–129

Tuckermann, D. B. and Pease, R. F. W. 1982. Optimized convective cooling using micromachined structures. *J. Electrochem. Soc.*, **129**, C98

Wang, B. X. and Peng, X. F. 1994. Experimental investigation on liquid forced-convection heat transfer through microchannels. *Int. J. Heat Mass Transfer*, **37** (suppl. 1), 73–82